Inorg. Chem. **2004**, *43*, 7844–7856

Synthesis and Characterization of a Chromium(V) *cis*-Dioxo Bis(1,10-phenanthroline) Complex and Crystal and Molecular Structures of Its Chromium(III) Precursor

Colin L. Weeks, Aviva Levina, Carolyn T. Dillon,† Peter Turner, Ronald R. Fenton, and Peter A. Lay*

Centre for Heavy Metals Research, School of Chemistry, University of Sydney, NSW 2006, Australia

Received July 22, 2004

The first structurally characterized Cr(V) dioxo complex, *cis*-$[Cr^{V}(O)_2(phen)_2](BF_4)$ (**2**, phen = 1,10-phenanthroline) has been synthesized by the oxidation of a related Cr(III) complex, *cis*-$[Cr^{III}(phen)_2(OH_2)_2](NO_3)_3 \cdot 2.5H_2O$ (**1**, characterized by X-ray crystallography), with NaOCl in aqueous solutions in the presence of excess $NaBF_4$, and its purity has been confirmed by electrospray mass spectrometry (ESMS), EPR spectroscopy, and analytical techniques. Previously reported methods for the generation of Cr(V)–phen complexes, such as the oxidation of **1** with PbO_2 or PhIO, have been shown by ESMS to lead to mixtures of Cr(III), Cr(V), Cr(VI), and in some cases Cr(IV) species, **3**. Species **3** was assigned as $[Cr^{IV}(O)(OH)(phen)_2]^+$, based on ESMS and X-ray absorption spectroscopy measurements. A distorted octahedral structure for **2** (Cr≡O, 1.63 Å; Cr–N, 2.04 and 2.16 Å) was established by multiple-scattering (MS) modeling of XAFS spectra (solid, 10 K). The validity of the model was verified by a good agreement between the results of MS XAFS fitting and X-ray crystallography for **1** (distorted octahedron; Cr–O, 1.95 Å; Cr–N, 2.06 Å). Unlike for the well-studied Cr(V) 2-hydroxycarboxylato complexes, **2** was equally or more stable in aqueous media (hours at pH = 1–13 and 25 °C) compared with polar aprotic solvents. A stable Cr(III)–Cr(VI) dimer, $[Cr^{III}(Cr^{VI}O_4)(phen)_2]^+$ (detected by ESMS), is formed during the decomposition of **2** in nonaqueous media. Comparative studies of the oxidation of **1** by NaOCl or PbO_2 have shown that $[Cr^{V}(O)_2(phen)_2]^+$ was the active species responsible for the previously reported oxidative DNA damage, bacterial mutagenicity, and increased incidence of micronuclei in mammalian cells, caused by the oxidation products of **1** with PbO_2. Efficient oxidation of **1** to a genotoxic species, $[Cr^{V}(O)_2(phen)_2]^+$, in neutral aqueous media by a biological oxidant, hypochlorite, supports the hypothesis on a significant role of reoxidation of Cr(III) complexes, formed during the intracellular reduction of Cr(VI), in Cr(VI)-induced carcinogenicity. Similar oxidation reactions may contribute to the reported adverse effects of a popular nutritional supplement, Cr(III) picolinate.

Introduction

Biological activities of Cr include well-established genotoxic, mutagenic, and carcinogenic actions of Cr(VI) compounds and a more controversial role of Cr(III) as an insulin potentiator in glucose and fat metabolism.[1] A generally accepted mechanism of Cr(VI)-induced genotoxicity[1] involves the following main steps: (i) the active transport of Cr(VI) into cells (through anion channels for soluble chromates or through phagocytosis for insoluble compounds such as $PbCrO_4$); (ii) the reduction of Cr(VI) within the cells or at the cell surface with the formation of potentially DNA-damaging Cr(V/IV) intermediates (which can be stabilized by intracellular ligands) and organic radicals; (iii) the formation of kinetically inert Cr(III) complexes, including highly genotoxic DNA−Cr(III)−protein and DNA−Cr(III)−DNA cross-links, as a result of such reduction. X-ray absorption spectroscopic (XAS) studies on single cells[2] have confirmed the predominance of the Cr(III) oxidation state

* Author to whom correspondence should be addressed. E-mail: p.lay@chem.usyd.edu.au.

† C.T.D. also has a position at the Australian Key Centre for Microscopy and Microanalysis and Electron Microscope Unit, Madsen Building, University of Sydney, NSW 2006, Australia.

(1) For a recent review, see: Levina, A.; Codd, R.; Dillon, C. T.; Lay, P. A. *Progr. Inorg. Chem.* **2003**, *51*, 145−250 and references therein.

(2) Dillon, C. T.; Lay, P. A.; Cholewa, M.; Legge, G. J. F.; Bonin, A. M.; Collins, T. J.; Kostka, K. L.; Shea-McCarthy, G. *Chem. Res. Toxicol.* **1997**, *10*, 533−535.

10.1021/ic049008q CCC: $27.50
Published on Web 10/28/2004

in Cr(VI)-treated mammalian cells. In contrast to Cr(VI), most Cr(III) complexes are noncytotoxic and nonmutagenic even at millimolar concentrations,[3] presumably due to the low cellular permeability related to their octahedral geometry and kinetic inertness.[4]

One of the less-studied aspects of Cr(VI)-induced genotoxicity is the possibility of intracellular reoxidation of Cr(III) complexes accumulated in Cr(VI)-treated cells.[1,5−7] Such reoxidation, involving reactive oxygen species formed by cellular redox enzymes, could potentially lead to genotoxic Cr(V/IV) complexes and be responsible for the long-term toxicity and carcinogenicity caused by the exposure to Cr(VI).[1,5−7] Furthermore, a recent hypothesis[7] related the reported antidiabetic activities of some Cr(III) complexes[8] to their intra- or extracellular oxidation to Cr(VI/V) species, which can act as phosphatase inhibitors by the mechanisms similar to that of a well-known insulin-mimetic V(V)[9] (isoelectronic to Cr(VI)). Thus, it was shown that dietary supplements could be oxidized to Cr(VI) by biological inorganic oxidants (H_2O_2, OCl^-) or by enzymatic oxidation and that the resultant Cr(VI) (and Cr(V)) are very efficient at inhibiting phosphatase enzymes in the same manner as V(V).[7a] Such enzyme inhibition is the postulated mechanism of the antidiabetic effect of V(IV/V) complexes.[9]

Complexes of Cr(III) with aromatic imine ligands, such as 1,10-phenanthroline (phen) or 2,2′-bipyridine (bpy), are among the few Cr(III) complexes that show a significant mutagenicity in bacterial assays;[6,10,11] this effect is strictly oxygen-dependent.[11] Initially, the mutagenicity of these Cr(III) compounds was attributed to their high lipophilicity, which makes them relatively permeable for the bacterial cells,[10] as well as to their reactions with cellular reductants, such as ascorbate.[11] Intracellular reduction of Cr(III) would lead to generation of unstable Cr(II) complexes, which then react with O_2 with the formation of DNA-damaging reactive oxygen species.[11] More recent studies[5,6] showed that the ability of some types of Cr(III) complexes to cause DNA damage and mutations in bacterial and mammalian cells strongly correlates with the ease of their oxidation to relatively stable Cr(V) complexes under biologically relevant conditions. For instance, oxidation of a mutagenic complex, *cis*-$[Cr^{III}(phen)_2(OH_2)_2]^{3+}$,[11] with PbO_2 in weakly acidic aqueous solutions causes the formation of a Cr(V) species (detected by EPR and electronic spectroscopies), which persists for hours at pH = 7.4 and 37 °C,[5,6] but the Cr(V) complex was not isolated or fully characterized. Comparative biological activity studies of the parent Cr(III) complex and its Cr(V)-containing oxidation product have shown that the formation of Cr(V) leads to significant increases in cellular permeability, cytotoxicity, and the incidence of micronuclei (in V79 Chinese hamster lung cells),[5] as well as in mutagenicity (in several strains of *Salmonella typhimurium*) and in oxidative DNA damage in vitro (plasmid DNA cleavage assay).[6]

The $[Cr^{III}(phen)_2(OH_2)_2](NO_3)_3$ complex was first synthesized in 1961[12] and was later assigned as a cis isomer on the basis of spectroscopic and X-ray powder diffraction studies,[13] but its crystal structure was not reported, although two related complexes, *cis*-$[Cr^{III}_2(phen)_4(\mu\text{-}OH)_2]Cl_4$ and *cis*-$[Cr^{III}(bpy)_2(OH_2)_2](NO_3)_3$, have been characterized by X-ray crystallography.[14,15] A solid isolated from the reaction of *cis*-$[Cr^{III}(phen)_2(OH_2)_2](NO_3)_3$ with PbO_2 in aqueous acetate buffers (pH = 4.0) by perchlorate precipitation was tentatively assigned as *cis*-$[Cr^{V}(O)_2(phen)_2](ClO_4)$, based on elemental analyses and IR spectroscopy.[16]

In the past decade, the use of electrospray mass spectrometry (ESMS) and X-ray absorption fine structure (XAFS) spectroscopy has led to structural characterizations of many unstable transition metal complexes, including several new Cr(V/IV) species.[1,17] In this work, the definitive characterization of the *cis*-$[Cr^{V}(O)_2(phen)_2]^+$ complex and the preliminary characterization of a Cr(IV)−phen complex are reported, as is the crystal structure of their Cr(III) analogue.

Experimental Section

Caution! *Cr(VI) compounds are human carcinogens,[18] and the Cr(V) and Cr(III)−phen complexes are mutagenic and potentially carcinogenic;[1,5,6] appropriate precautions should be taken to avoid skin contact and inhalation of their solutions and dusts. Perchlorate salts of Cr(III) complexes are potentially explosive; only small quantities of the solids (<0.1 g) should be handled with plastic spatula.*

Reagents and Solutions. The following commercial reagents of analytical or higher purity were used without purification: boron nitride (BN), 2-ethyl-2-hydroxybutanoic acid, ferrocene, iodobenzene diacetate, 1,10-phenanthroline monohydrate, (^{n}Bu$_4$N)BF$_4$,

(3) De Flora, S.; Camoirano, A.; Bagnasco, M.; Zanacchi, P. In *Handbook of Metal−Ligand Interactions in Biological Fluids. Bioinorganic Medicine*; Berthon, G., Ed.; Marcel Dekker: New York, 1995; Vol. 2, pp 1020−1036.
(4) Lay, P. A.; Levina, A. In *Comprehensive Coordination Chemistry II*; McCleverty, J. A., Meyer T. J., Eds.; Elsevier: Oxford, U.K., 2004; Vol. 4, pp 313−413.
(5) Dillon, C. T.; Lay, P. A.; Bonin, A. M.; Cholewa, M.; Legge, G. J. F. *Chem. Res. Toxicol.* **2000**, *13*, 742−748.
(6) Dillon, C. T.; Lay, P. A.; Bonin, A. M.; Dixon, N. E.; Sulfab, Y. *Aust. J. Chem.* **2000**, *53*, 411−424.
(7) (a) Mulyani, I.; Levina, A.; Lay, P. A. *Angew. Chem., Int. Ed.* **2004**, *43*, 4504−4507. (b) Levina, A.; Lay, P. A. *Coord. Chem. Rev.* **2004**, in press.
(8) Vincent, J. B. *J. Trace Elem. Exp. Med.* **2003**, *16*, 227−236 and references therein.
(9) (a) Stankiewicz, P. J.; Tracey, A. S.; Crans, D. C. In *Metal Ions in Biological Systems, Vol. 31*; Sigel, H., Sigel, A., Eds.; Marcel Dekker: New York, 1995; pp 287−324. (b) Zhang, M.; Zhou, M.; Van Etten, R. L.; Stauffacher, C. V. *Biochemistry* **1997**, *36*, 15−23.
(10) Warren, G.; Schultz, P.; Bancroft, D.; Bennett, K.; Abbott, E. H.; Rogers, S. *Mutat. Res.* **1981**, *90*, 111−118.
(11) (a) Sugden, K. D.; Burris, R. B.; Rogers, S. J. *Mutat. Res.* **1990**, *244*, 239−244. (b) Sugden, K. D.; Geer, R. D.; Rogers, S. J. *Biochemistry* **1992**, *31*, 11626−11631.
(12) Inskeep, R. G.; Bjerrum, J. *Acta Chem. Scand.* **1961**, *15*, 62−68.
(13) (a) Inskeep, R. G.; Benson, M. *J. Inorg. Nucl. Chem.* **1961**, *20*, 290−294. (b) Andersen, P.; Josephsen, J. *Acta Chem. Scand.* **1971**, *25*, 3255−3260. (c) Hancock, M. P.; Josephsen, J.; Schaeffer, C. E. *Acta Chem. Scand. A* **1976**, *30A*, 79−97.
(14) Veal, J. T.; Hatfield , W. E.; Hodgson, D. J. *Acta Crystallogr. B* **1973**, *29*, 12−20.
(15) Casellato, U.; Graziani, R.; Maccarrone, G.; Di Bilio, A. J. *J. Crystallogr. Spectrosc. Res.* **1986**, *16*, 695−702.
(16) Sulfab, Y.; Nasreldin, M. *Transition Met. Chem.* **2001**, *26*, 147−149.
(17) Levina, A.; Armstrong, R. S.; Lay, P. A. *Coord. Chem. Rev.* **2004**, in press.
(18) *IARC. Monographs on the Evaluation of the Carcinogenic Risk of Chemicals to Humans. Vol. 49. Chromium, Nickel and Welding*; International Agency on the Research of Cancer: Lyon, France, 1990.

NaOCl (aqueous solution, ≥4% of active Cl), and NaOH (99.99%) from Aldrich; *sym*-diphenylcarbazide from Fluka; L-ascorbic acid from ICN Biomedicals; D-glucose, sulfolane (tetramethylene-sulfone), $Cr(NO_3)_3 \cdot 9H_2O$, CH_3COOH, HCl (35% w/v in H_2O), HNO_3 (69% w/v in H_2O, trace pure), KBr, $LiClO_4$, $NaBF_4$, $NaClO_4$, $Na_2CrO_4 \cdot 4H_2O$, $NaH_2PO_4 \cdot H_2O$, NH_3 (32% w/v in H_2O), and PbO_2 from Merck; *N*-(2-hydroxyethyl)-piperazine-*N*′-(2-ethanesulfonic acid) (HEPES) from Research Organics; glutathione (reduced form) from Sigma. The following HPLC grade solvents (from Aldrich) were used without purification: acetone, acetonitrile, diethyl ether, *N*,*N*-dimethylformamide (DMF), dimethyl sulfoxide (DMSO), and methanol. Water was purified by the Milli-Q technique. Iodosobenzene (PhIO) was synthesized by the reaction of $PhI(OAc)_2$ with aqueous NaOH[19] and stored at 4 °C. Concentrations of NaOCl in the commercial solution were determined at the day of experiment from the absorbance at 292 nm ($\epsilon = 3.5 \times 10^2$ M^{-1} cm^{-1} at pH = 12).[20] Stock solutions of the buffers were treated by Chelex 100 chelating resin (BioRad) and stored at 4 °C. Working solutions of the buffers were prepared daily by adjusting the pH values of the stock solutions with high-purity NaOH or NH_3; the pH values were measured by an Activon 210 ionometer with an AEP 321 glass/calomel electrode. Concentrations of the catalytic metals (Fe(III) and Cu(II)) in the buffers, determined by Buettner's ascorbate method,[21] were <0.5 μM.

Syntheses of Cr Complexes. The synthesis of *cis*-$[Cr^{III}(phen)_2(OH_2)_2](NO_3)_3 \cdot 2.5H_2O$ (**1**) was performed according to the literature method.[12,13a] Recrystallization of the product from 0.10 M HNO_3 yielded dark orange needles. Anal. Calcd for $C_{24}H_{25}CrN_7O_{13.5}$: Cr, 7.66; C, 42.42; H, 3.71; N, 14.43. Found: Cr, 7.8; C, 42.60; H, 3.68; N, 14.38. UV−vis (0.10 M HNO_3): 498 nm (39 M^{-1} cm^{-1}); lit.[13a] UV−vis 497 nm (41 M^{-1} cm^{-1}).

For the synthesis of *cis*-$[Cr^{V}(O)_2(phen)_2]BF_4 \cdot 0.3Et_2O$ (**2**), **1** (136 mg, 0.200 mmol) and $NaBF_4$ (300 mg, 2.73 mmol) were dissolved in H_2O (20 mL), and the solution was cooled to ∼4 °C. Addition of NaOCl (1.43 mL of 0.705 M solution, 1.01 mmol) resulted in immediate formation of a fine yellow precipitate, which was separated by centrifugation (5 min at 4000*g*, 4 °C), washed twice with ice-cold water (10 mL) and then with Et_2O (10 mL), and dried under vacuum (24 h at 25 °C). Yield: 92 mg (83%). The precipitate could also be separated by vacuum filtration on a microporous glass filter, but the yield then decreased to ∼30% due to incomplete retention of the precipitate. Anal. Calcd for $C_{25.2}H_{19}N_4O_{2.3}CrBF_4$: Cr, 9.40; C, 54.7; H, 3.46; N, 10.13. Found: Cr, 9.3; C, 54.8, H, 3.33, N, 10.46. TGA: mass loss 3.8% at 100−120 °C. ESMS (MeCN, +ve ion): *m*/*z* 444.1. UV−vis (MeCN): 410 nm (6.9×10^2 M^{-1} cm^{-1}). EPR (MeCN): $g_{iso} = 1.9357$. Magnetic moment (solid, 295 K): $\mu_{eff} = 1.89$ μ_B. IR (KBr matrix): 3591 w, br, 3452 w, br, 3062 w, br, 1628 w, 1605 w, 1583 w, 1518 m, 1427 m, 1342 w, 1308 w, 1226 w, 1143 m, 1062 s, 873 m, 849 s, 724 s, 649 w, 521 w, 428 cm^{-1} w. The product is soluble (10−25 mM) in polar aprotic solvents (MeCN, DMF, DMSO, or sulfolane) and slightly soluble (∼0.20 mM) in H_2O at 25 °C. For preparation of aqueous solutions of **2** (typically, 1.0 mM), freshly prepared solutions in MeCN (20 mM) were diluted with H_2O or aqueous buffers.

Isolation of the oxidation products formed in the reaction of **1** with PbO_2 was carried out as described before (although no exact conditions were specified).[16] Typically, **1** (30 mg, 0.044 mmol) was dissolved in acetate buffer (2.0 mL, 50 mM, pH = 4.0) and sonicated with PbO_2 (80 mg, 0.33 mmol) for 10 min at 25 °C. The resulting suspension was filtered through a 0.20-μm cellulose-membrane filter (Sartorius), and $NaClO_4$ (20 mg, 0.16 mmol) was added to the filtrate. The resulting yellow precipitate was separated by vacuum filtration on a glass filter, washed with ice-cold H_2O and then with Et_2O, and dried under vacuum (yield, 15 mg).

A typical procedure for the isolation of oxidation products formed in the reaction of **1** with PhIO was as follows. A mixture of **1** (100 mg, 0.147 mmol) and PhIO (55 mg, 0.25 mmol) was dissolved with stirring (15 min at 25 °C) in a mixture of MeCN (20 mL) and DMF (5.0 mL). To the resulting solution was added $LiClO_4$ (61 mg, 0.57 mmol), followed by the addition of Et_2O (50 mL). After 5−10 min at 25 °C, a small amount of dark-red oily precipitate was formed on the walls of the flask. The precipitate was separated by decanting the solvent, rinsing the walls of the flask with Et_2O (which did not remove the precipitate), and drying under vacuum (yield, 7.0 mg). The isolated solid was shown by XAS and ESMS (see Results) to consist predominantly of a Cr(IV) complex, $[Cr^{IV}O(OH)(phen)_2](ClO_4)$ (**3**).

A well-characterized Cr(V) complex, $Na[Cr^{V}O(ehba)_2] \cdot 1.5H_2O$ ($ehbaH_2$ = 2-ethyl-2-hydroxybutanoic acid),[22] was synthesized by a literature method,[23] and its purity was confirmed by electronic and EPR spectroscopies (for 1.0 mM solution in DMF, $\epsilon_{510} = 1.7 \times 10^2$ M^{-1} cm^{-1}, $g_{iso} = 1.9782$, and $A_{iso}(^{53}Cr) = 17.1 \times 10^{-4}$ cm^{-1}).[22,23]

Analytical Techniques. The Cr contents of **1** and **2** were determined (after digestion of the samples with 69% HNO_3) by C_2H_2/air flame atomic absorption spectroscopy, using a Varian SpecAA-800 spectrometer, calibrated with standard Cr(III) solutions (Aldrich). Elemental analyses (C, H, N) were performed by the Australian National University Microanalytical Unit, using a Carlo Erba 1106 automatic analyzer. Thermogravimetric analyses (TGA) were performed on a TGA 2950 analyzer (TA Instruments) by heating the samples in an atmosphere of high-purity N_2 (BOC gases) from 20 to 250 °C at 1.0 °C/min. Magnetic susceptibility was measured on a Sherwood Scientific magnetic balance, calibrated with $(NH_4)_2Fe(SO_4)_2 \cdot 6H_2O$, and diamagnetic corrections for the constituent atoms were calculated from the literature.[24] Solid-state IR spectra were recorded using a diffuse reflectance technique (for the mixtures with KBr) on a BioRad FTS-40 spectrometer. Cyclic voltammetry experiments were performed using a Bioanalytical Systems BAS 100B electrochemical analyzer (scan rate, 100 mV s^{-1}; 100% *iR* compensation) with a glassy carbon working electrode (3.0-mm diameter), a Ag/AgCl reference electrode, filled with 3.0 M aqueous NaCl, Pt wire as an auxiliary electrode, and ferrocene (Fc) as an internal standard. Electrochemical measurements were carried out in MeCN solutions, containing $(^nBu_4N)BF_4$ (0.10 M) as the supporting electrolyte, and saturated with O_2-free Ar (BOC gases). Electronic absorption spectra (UV−vis; λ = 300−800 nm; resolution, 2.0 nm; integration time, 0.20 s) were acquired on a Hewlett-Packard HP 8452 A diode-array spectrophotometer.

Concentrations of Cr(VI) in the decomposition products of **2** were determined spectrophotometrically with diphenylcarbazide (DPC, $\epsilon = 4.2 \times 10^4$ M^{-1} cm^{-1} at 540 nm),[25] as described previously,[26] and calibrations were performed by a standard additions method.

(19) Saltzman, H.; Sharefkin, J. G. In *Organic Syntheses*; Baumgarten, H. E., Ed.; John Wiley and Sons: New York, 1973; Collect. Vol. 5, pp 658−659.
(20) Morris, J. C. *J. Phys. Chem.* **1966**, *70*, 3798−3805.
(21) Buettner, G. R. *Methods Enzymol.* **1990**, *186*, 125−127.
(22) Judd, R. J.; Hambley, T. W.; Lay, P. A. *J. Chem. Soc., Dalton Trans.* **1989**, 2205−2210.
(23) Krumpolc, M.; Roček, J. *J. Am. Chem. Soc.* **1979**, *101*, 3206−3209.
(24) Mabbs, F. E.; Machin, D. J. *Magnetism and Transition Metal Complexes*; Chapman and Hall: London, 1973.
(25) *Standard Methods for the Examination of Water and Wastewater*, 19th ed.; American Public Health Association: Washington, DC, 1995; pp 3.59−3.60.

In a typical experiment, a solution of DPC (40 mM in DMSO, 10 μL) and a decomposed solution of **2** in H_2O or organic solvent ([Cr] = 1.0 mM, 10 μL) were added to an aqueous HCl solution (0.10 M, 0.98 mL), and the absorbance at 540 nm was followed for 30 min at 25 °C (measured every 15 s). In control experiments, no significant effects of added organic solvents (up to 10% vol) on the determination of Cr(VI) by the DPC methods were observed.

Solid-state and solution EPR spectra (X-band) were acquired on a Bruker EMX spectrometer, using quartz capillaries (solid state) and Wilmad quartz flat cell (solutions); calibrations of the magnetic field and the microwave frequency were performed with an EMX 035 NMR gaussmeter and an EMX 048T microwave bridge controller, respectively. Typical instrumental settings were as follows: center field, 3500 G; sweep width, 6900 G (solids) or 200 G (solutions); resolution, 1024 points; microwave power, 2.0 mW; microwave frequency, ~9.78 GHz (solids) or ~9.67 GHz (solutions); modulation frequency, 100 kHz; modulation amplitude, 5.0 G (solids) or 1.0 G (solutions); time constant, 20.48 ms; receiver gain, 10^2−10^5; number of scans, 5. The EPR spectra were processed with WinEPR software;[27] second-order corrections were applied in the determinations of the g_{iso} and A_{iso} values.

The ESMS analyses were performed using a Finnigan LCQ mass spectrometer; typical experimental settings were as follows: sheath gas (N_2) pressure, 60 psi; spray voltage, 4.0 kV; capillary temperature, 150 °C; cone voltage, 3.0 V (positive-ion mode) or 25 V (negative-ion mode); tube lens offset, 20 V; *m*/*z* range, 100−2000 (both in positive- and negative-ion modes). Mild ESMS conditions in the positive-ion mode (listed above) were required to minimize the gas-phase reactions of the studied complexes (see Results). For some systems, positive-ion ESMS were also acquired at harsher conditions: capillary temperature, 200 °C; cone voltage, 25 V; other parameters were as indicated above. Analyzed solutions (5.0 μL, 1.0 mM Cr) were injected into a flow of H_2O/MeOH (1:1 v/v, flow rate 0.20 mL min^{-1}). Acquired spectra were the averages of 10 scans (scan time 10 ms). Unless stated otherwise, no significant signals were detected in the negative-ion mode (apart from those of BF_4^-), as well as in the positive-ion mode in the *m*/*z* = 1000−2000 range. Simulations of the mass spectra were performed using IsoPro software.[28]

All the analytical results were reproduced in at least two independent experimental series, using different sets of stock solutions and different preparations of **1** and **2**; relative deviations in the results of parallel experiments did not exceed 10%.

X-ray Absorption Spectroscopy and Data Processing. Chromium K-edge spectra of **1**−**3** were recorded on the Australian National Beamline Facility (beamline 20B) at the Photon Factory, Tsukuba, Japan. The beam energy was 2.5 GeV, and the beam current, 300−400 mA. A Si[111] double-crystal monochromator was detuned by 50%. The spectra were recorded in transmission mode, using N_2/He-filled ionization chambers. Solid samples were mixed with BN (~1:1 w/w) and pressed into 0.5-mm pellets supported in an Al spacer between two 63.5-μm Kapton tape windows. The sample temperature was maintained at 10 ± 1 K using a closed-cycle He CryoIndustries REF-1577-D22 cryostat. Collection of XAS data at low-temperature minimized sample photodamage, improved the signal-to-noise ratio, and maximized the multiple-scattering (MS) contributions to the XAFS spectrum.[29] The spectra were averaged from three scans taken at different positions on the sample; no color changes at irradiated spots were observed, and the edge energies differed by <0.1 eV between the scans. The energy scale was calibrated using a Cr foil as an internal standard (calibration energy, 5989.0 eV, corresponded to the first peak of the first derivative of Cr(0) edge).[30] Averaging, background subtraction, and the calculations of theoretical XAFS spectra, were performed using the XFIT software package,[30] including FEFF 4.06[31] and FEFF 6.01[32] algorithms, as described previously.[29] Detailed descriptions of the applied single-scattering (SS) and MS XAFS models are given in the Results. The determinacies (N_i/p, where N_i is the number of independent observations and p is the number of varied parameters) of the models used in SS and MS XAFS calculations were estimated by the method of Binsted et al.,[33] taking into account the applied restraints and constraints. Overdetermined models ($N_i/p > 1$) were used in XAFS calculations, which allowed meaningful solutions to be obtained.[33] The goodness-of-fit parameters for XAFS fittings using different models were compared using a statistical *F*-test.[34,35] The random errors in the estimated XAFS parameters, arising from the noise in the data, were determined by Monte Carlo analysis within the XFIT software.[30] Starting coordinate sets for MS XAFS calculations were obtained from the X-ray crystal structure of **1**.

X-ray Crystallography. An orange columnar crystal of **1** was attached to a thin glass fiber and mounted on a Bruker SMART 1000 CCD diffractometer employing graphite-monochromated Mo Kα radiation generated from a sealed tube. Cell constants were obtained from a least-squares refinement against 4587 reflections located between 4.42 and 51.77° in 2θ. Data were collected at 297(2) K with ω scans to 56.00° in 2θ, and the full sphere coverage was 0.99. The intensities of 339 standard reflections recollected at the end of the experiment did not change significantly during the data collection. An empirical absorption correction determined with SADABS[36,37] was applied to the data. The data integration and reduction were undertaken with SAINT and XPREP,[38] and subsequent computations were carried out with the teXsan[39] graphical user interface. The structure was solved in the space group $Pna2_1$ (No. 33) by direct methods with SIR97[40] and extended and refined with SHELXL-97,[41] and plots were drawn using ORTEP.[42] The

(26) Levina, A.; Bailey, A. M.; Champion, G.; Lay, P. A. *J. Am. Chem. Soc.* **2000**, *122*, 6208−6216.
(27) *WinEPR, Version 960801*; Bruker-Franzen Analytic: Bremen, Germany, 1996.
(28) Published by author: Senko, M. *IsoPro 3.0*; Sunnyvale, CA, 1998.
(29) (a) Rich, A. M.; Armstrong, R. S.; Ellis, P. J.; Freeman, H. C.; Lay, P. A. *Inorg. Chem.* **1998**, *37*, 5743−5753. (b) Rich, A. M.; Armstrong, R. S.; Ellis, P. J.; Lay, P. A. *J. Am. Chem. Soc.* **1998**, *120*, 10827−10836.
(30) (a) Ellis, P. J.; Freeman, H. C. *J. Synchrotron Radiat.* **1995**, *2*, 190−195. (b) *XFIT for Windows'95*; Australian Synchrotron Research Program: Sydney, Australia, 1996.
(31) Mustre de Leon, J.; Rehr, J. J.; Zabinsky, S. I.; Albers, R. C. *Phys. Rev. B.* **1991**, *44*, 4146−4156.
(32) Rehr, J. J.; Albers, R. C.; Zabinsky, S. I. *Phys. Rev. Lett.* **1992**, *69*, 3397−3400.
(33) Binsted, N.; Strange, R. W.; Hasnain, S. S. *Biochemistry* **1992**, *31*, 12117−12125.
(34) Neville, A. M.; Kennedy, J. B. *Basic Statistical Methods for Engineers and Scientists*; International Textbook Co.: Scranton, PA, 1966; pp 312−313.
(35) Levina, A.; Lay, P. A. *Inorg. Chem.* **2004**, *43*, 324−335.
(36) Blessing, R. H. *Acta Crystallogr. A* **1995**, *51*, 33−38.
(37) Sheldrick, G. M. *SADABS. Empirical Absorption Correction Program for Area Detector Data*; University of Göttingen: Göttingen, Germany, 1996.
(38) *SMART, SAINT and XPREP. Area Detector Control and Data Integration and Reduction Software*; Bruker Analytical X-ray Instruments Inc.: Madison, WI, 1995.
(39) *teXsan for Windows: Single-Crystal Structure Analysis Software*; Molecular Structure Corp.: The Woodlands, TX 77381, 1997−1998.
(40) Altomare, A.; Burla, M. C.; Camalli, M.; Cascarano, G. L.; Giacovazzo, C.; Guagliardi, A.; Moliterni, A. G. G.; Polidori, G.; Spagna, R. *J. Appl. Crystallogr.* **1998**, *32*, 115−119.
(41) Sheldrick, G. M. *SHELXL97. Program for Crystal Structure Refinement*; University of Göttingen: Göttingen, Germany, 1997.

Table 1. Summary of Crystal Data and Structure Refinement Details for **1**

formula of the refinement model	$C_{24}H_{24}CrN_7O_{13.5}$
model M_r	678.50
cryst system	orthorhombic
space group	$Pna2_1$ (No. 33)
a	9.5923(5) Å
b	32.8173(16) Å
c	9.0928(5) Å
V	2862.4(3) Å^3
D_c	1.574 g cm^{-3}
Z	4
cryst size	0.394 × 0.085 × 0.07 mm
cryst color	orange
cryst habit	columnar
λ(Mo Kα)	0.71073 Å
μ(Mo Kα)	0.482 cm^{-1}
T(SADABS)$_{min,max}$	0.899, 1.000
$2\theta_{max}$	56.00°
hkl range	−12/12, −41/43, −11/11
N	26 316
N_{ind}	6669 (R_{merge} = 0.0258)
N_{obs}	5788 [$I > 2\sigma(I)$]
N_{var}	442
resids[a] R1(F), wR2(F^2)	0.0364, 0.0953

[a] $R1 = \Sigma||F_o| - |F_c||/\Sigma|F_o|$ for $F_o > 2\sigma(F_o)$; $wR2 = (\Sigma w(F_o^2 - F_c^2)^2/\Sigma(wF_c^2)^2)^{1/2}$ for all reflections; $w = 1/[\sigma^2(F_o^2) + (0.0580P)^2 + 0.1742P]$, where $P = (F_o^2 + 2F_c^2)/3$.

asymmetric unit contains the complex molecule, three nitrate ions, and three solvate water molecules. One of the water molecule sites was modeled with a 50% site occupancy and isotropic thermal parameters. The other non-hydrogen atoms were modeled with anisotropic displacement parameters. The hydrogen atoms of the full occupancy water molecules were located and refined; no hydrogens were included in the model for the partial occupancy water molecule. A riding atom model was used for the rest of the hydrogen atoms. The absolute structure was established with the Flack parameter[43,44] refining to −0.009(15). The crystal data and refinement details are summarized in Table 1.

Results

X-ray Crystallography of 1. The X-ray crystal structure of **1** (Figure 1 and Table 2) confirmed the cis coordination geometry of this complex, with the average Cr−O and Cr−N bond lengths of 1.95 and 2.06 Å, respectively. These values are consistent with those for the Cr−O bonds in $[Cr(OH_2)_6](NO_3)_3$ (1.95−1.97 Å),[45] the Cr−N bonds in $[Cr(phen)_3](ClO_4)_3$ (2.040−2.055 Å),[46] and the corresponding bond lengths in *cis*-$[Cr(bpy)_2(OH_2)_2](NO_3)_3$, where the Cr−O bond lengths are 1.98 and 2.00 Å and the Cr−N_{av} bond length is 2.04 Å.[14] There is a hydrogen-bonded network involving the coordinated water molecules, the nitrate counterions, and the water solvate molecules (Figure 2). The complex molecule itself has a noncrystallographic 2-fold axis passing through the metal ion and bisecting the water−metal−water angle. The coordination of the Cr center is pseudooctahedral; the deviation from octahedral geometry is mainly due to the N−Cr−N angles of the phen ligands being ∼80° (Table 2). Only the Λ-enantiomer in the racemic crystals of **1** (Chart 1)[47] is displayed in the figures.

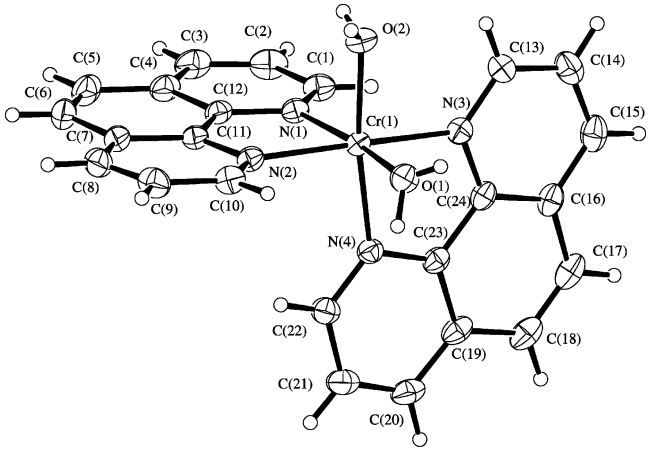

Figure 1. ORTEP[42] depiction of the Λ-enantiomer of the cation in the crystal structure of **1**, which shows 25% atom displacement ellipsoids.

Table 2. Selected Structural Data for **1**−**3**

atoms[a]	**1** (XRD)[b]	**1** (XAFS)[c]	**2** (XAFS)[c,d]	**3** (XAFS)[e]
		Bond Lengths (Å)		
Cr−O(1)	1.959(2)	1.94	1.63	1.54
Cr−O(2)	1.953(2)	1.94	1.63	1.70
Cr−N(1)	2.067(2)	2.04	2.04	2.02
Cr−N(2)	2.063(2)	2.07	2.16	2.02
Cr−N(3)	2.064(2)	2.07	2.16	2.02
Cr−N(4)	2.059(2)	2.04	2.04	2.02
		Bond Angles (deg)		
O(1)−Cr−O(2)	88.62(9)	89	112	
O(1)−Cr−N(1)	172.11(9)	171	163	
O(1)−Cr−N(2)	91.79(9)	94	93	
O(2)−Cr−N(1)	91.90(8)	96	84	
O(2)−Cr−N(2)	91.04(8)	88	104	
N(1)−Cr−N(2)	80.33(7)	79	79	
N(1)−Cr−N(3)	93.12(8)	91	94	
N(1)−Cr−N(4)	91.08(7)	95	80	
N(2)−Cr−N(3)	172.67(8)	171	170	

[a] Atomic numbering corresponds to Figure 1. [b] Determined by X-ray diffraction (see the CIF file in the Supporting Information for details); errors in the last significant figures are shown in parentheses. [c] Determined by MS XAFS fittings (see Tables S5−S7 in the Supporting Information for details). Errors in the optimized parameters, arising from the noise in experimental data (determined by Monte Carlo analyses),[30] were ≤0.007 Å for the bond lengths and ≤1° for the bond angles, and conservative estimates of the systematic errors were 0.01−0.02 Å and 1−2°, respectively.[29,30] [d] Corresponds to model **2a** in Chart 1 and Table S6. [e] Determined by single scattering (SS) XAFS fittings (see Table S4 in the Supporting Information for details).

Synthesis of 2 by Oxidation of 1 with NaOCl. Reactions of **1** with oxidants were conveniently followed by ESMS. Some typical mass spectra and separate signals are shown in Figure 3, and the following data are placed in Supporting Information: (i) typical wide-scan spectra (m/z = 100−1000, Figures S1−S6); (ii) typical experimental and simulated isotopic distributions (Figure S7, other than those shown in Figure 3); (iii) the assignment of the major ESMS signals (Table S1). The main ESMS signal for aqueous solutions of **1** (pH ∼ 6) is that of a doubly deprotonated species, $[Cr^{III}(OH)_2(phen)_2]^+$ (m/z = 446.1, Figures 3a and S1a).

(42) Johnson, C. K. *ORTEPII, A Thermal Ellipsoid Plotting Program*; Oak Ridge National Laboratories: Oak Ridge, TN, 1976.
(43) Flack, H. D. *Acta Crystallogr. A* **1983**, *39*, 876−881.
(44) Bernadelli, G.; Flack, H. D. *Acta Crystallogr. A* **1985**, *41*, 500−511.
(45) Lazar, D.; Ribar, B.; Divjakovic, V.; Meszaros, C. *Acta Crystallogr. C* **1991**, *47*, 1060−1062.
(46) Luck, R. L.; Gawryszewska, P.; Riehl, J. P. *Acta Crystallogr. C* **2000**, *56*, e238−e239.
(47) Cotton, F. A.; Wilkinson, G. *Advanced Inorganic Chemistry*, 5th ed.; John Wiley and Sons: New York, 1988; pp 638−647.

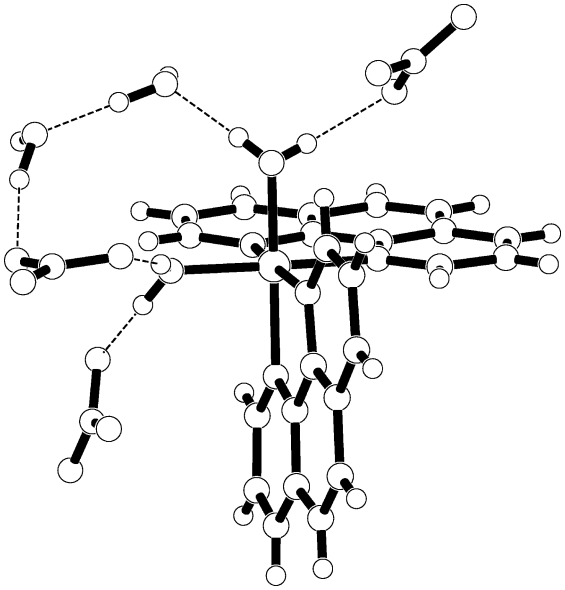

Figure 2. Hydrogen-bonding network in the crystal structure of **1**.

Chart 1. Outlines of the Structures of **1**−**3**, Refined by XAFS Calculations (Table 2)[a]

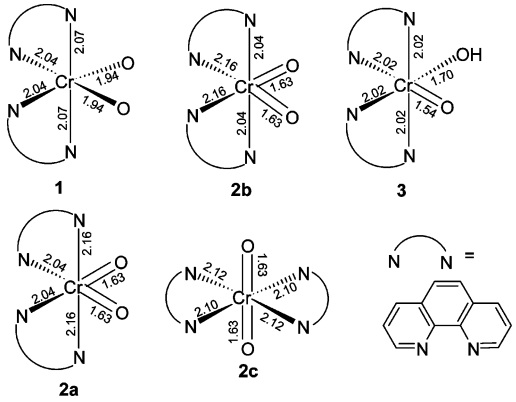

[a] The numbers on the bonds show the bond lengths in Å.

Deprotonation of **1** to $[Cr^{III}(OH)(OH_2)(phen)_2]^{2+}$ is known to occur in neutral aqueous solutions.[6,13] Further deprotonation occurs in the gas phase under the ESMS conditions, which are known to favor the existence of single-charged over multiple-charged ions.[48] Formation of Cr(V) after the addition of NaOCl is manifested by the appearance of a signal at $m/z = 444.1$ due to $[Cr^{V}(O)_2(phen)_2]^+$ (Figures 3b and S1b), as well as by an increase in absorbance at 350−600 nm in electronic spectra (Figure S8a in Supporting Information) and the appearance of an EPR signal at $g_{iso} = 1.9386$, as reported previously for the oxidation of **1** with PbO_2.[6,49] A combination of ESMS and electronic absorption spectroscopy was used to find the optimal conditions for quantitative generation of $[Cr^{V}(O)_2(phen)_2]^+$ in solutions ([**1**] = 10 mM and [NaOCl] = 50 mM in unbuffered H_2O); the reaction is complete within <15 s at 25 °C. The release of protons during the oxidation of $[Cr^{III}(phen)_2(OH_2)_2]^{3+}$ to $[Cr^{V}(O)_2(phen)_2]^+$ led to an increase in acidity from pH ∼ 6

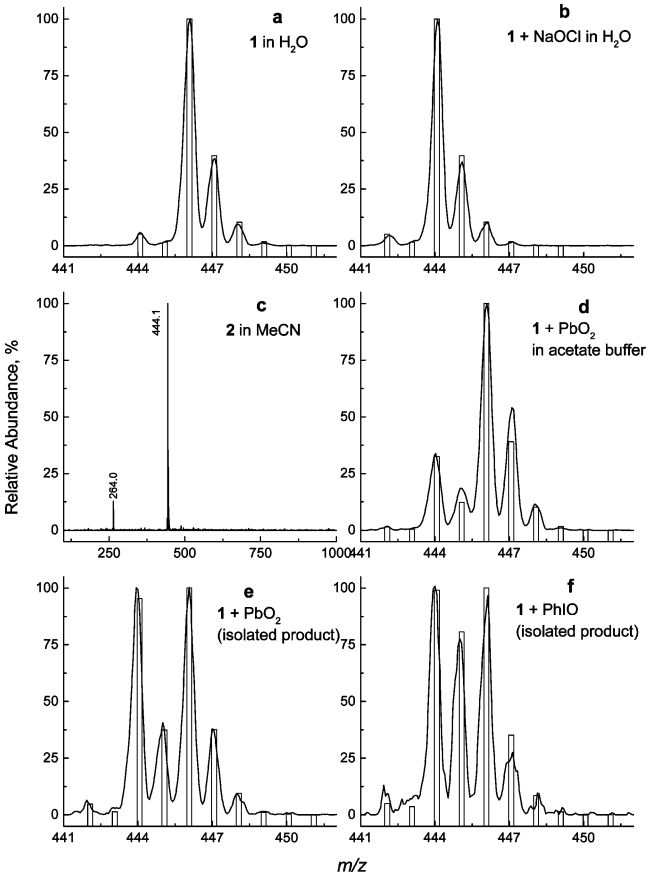

Figure 3. Typical ESMS data in the positive-ion mode ([Cr] ∼ 1.0 mM; full scan for c and expanded signals for a and b and d−f; lines, experimental data; columns, simulated data) for **1** and its oxidation products. Conditions: capillary temperature, 150 °C; cone voltage, 3.0 V; other ESMS parameters as given in the Experimental Section. Experimental details and simulation results are given in the text, and full scans for a and b and d−f are given in Figures S1−S3, Supporting Information.

to pH ∼ 2. Higher concentrations of **1**, as well as lower [NaOCl]/[**1**] ratios, led to precipitation of partially oxidized products. No significant decomposition of the formed Cr(V) species was observed (by ESMS and electronic spectroscopy) for at least 15 min at 25 °C. Thus, the synthesis of **2** (see Experimental Section) was performed under the conditions leading to quantitative generation of Cr(V). In addition, the use of BF_4^- as a counterion ensured the selective precipitation of **2**, since the addition of $NaBF_4$ (0.14 M) to aqueous solutions of **1** (10 mM) did not lead to any precipitation.

The results of elemental analyses and TGA (see Experimental Section) were consistent with the formulation of the isolated solid **2** as $[Cr^{V}(O)_2(phen)_2](BF_4)\cdot 0.3Et_2O$, and the presence of two oxo groups in a cis geometry ($\nu = 839$ and 873 cm^{-1})[16] was confirmed by IR spectroscopy (Figure S9 in Supporting Information). The magnetic moment of **2** at 295 K ($\mu_{eff} = 1.89\ \mu_B$) was slightly higher than the spin-only value for a Cr(V) (d^1) complex (1.73 μ_B)[24] but lower than the value for $Na[Cr^{V}O(ehba)_2]$ (2.05 μ_B).[23] The main signal observed in the ESMS of **2** (1.0 mM solution in MeCN, Figure 3c) was that of $[Cr^{V}(O)_2(phen)_2]^+$ at $m/z = 444.1$ (the expanded signal was identical with that in Figure 3b). The appearance of $[Cr^{V}(O)_2(phen)]^+$ ($m/z = 264.0$, Figures 3c and S7) as a minor species was due to the

(48) (a) Gaskell, S. J. *J. Mass Spectrom.* **1997**, *32*, 677−688. (b) Cole, R. B. *J. Mass Spectrom.* **2000**, *35*, 763−772.

(49) An erroneous value of g_{iso} for $[Cr^{V}(O)_2(phen)_2]^+$ (1.972 in aqueous solutions) was reported in ref 16.

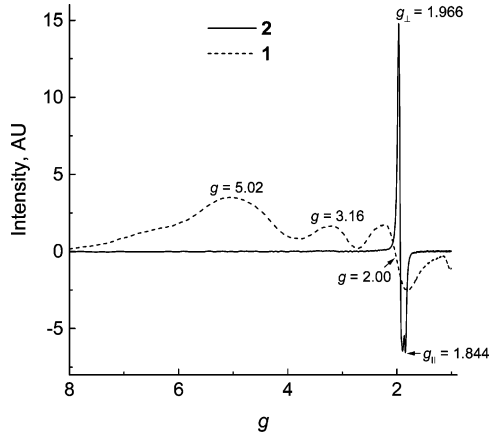

Figure 4. Solid-state X-band EPR spectra of **1** and **2** at 25 °C.

Table 3. EPR Spectra and Stability of **2** in Solutions[a]

solvent	g_{iso}	10^4LW,[b] cm^{-1}	$t_{1/2}$,[c] s	Cr(VI),[d] mol %
MeCN	1.9357	32.5	1.2×10^4	26
DMF	1.9367	35.2	9.8×10^2	24
DMSO	1.9376	45.7	8.0×10^2	45
sulfolane[e]	1.9508	67.9	4.6×10^3	52
H_2O (pH = 5.2)[f,g]	1.9386	31.9	1.8×10^4	57
NaOH (0.10 M)[g]	1.9386	31.4	1.1×10^4	59
HCl (0.10 M)[g]	1.9386	33.0	3.4×10^3	15

[a] All the experiments were performed at [Cr] = 1.0 mM and 25 ± 1 °C. [b] Line width of the EPR signal. [c] Half-life time of the Cr(V) complex (1.0 mM), measured by EPR and/or electronic absorption spectroscopies. [d] Amount of Cr(VI) (relative to total Cr) formed during the decomposition of **2** ($t \sim 10t_{1/2}$). [e] Measurements in sulfolane (melting point 27 °C) were performed at 30 ± 1 °C. [f] Similar results (within 15% experimental error) were obtained in aqueous buffer solutions: phosphate (0.10 M, pH = 7.4) and acetate (0.10 M, pH = 4.0). [g] Aqueous solutions, containing MeCN (5% v/v, used for complete dissolution of **2**).

dissociation of one phen ligand from the parent complex under the ESMS conditions, since a dramatic increase in the relative abundance of this species was observed with an increase in capillary temperature and cone voltage (Figure S2a in Supporting Information).

Solid-state X-band EPR spectroscopy of **2** at 25 °C (Figure 4) showed a sharp anisotropic signal due to Cr(V) ($g_\parallel = 1.844$ and $g_\perp = 1.966$) and did not reveal any traces of **1**. The latter complex possessed broad EPR signals at $g = 2.00$, 3.16, and 5.02 (Figure 4), in agreement with the literature data.[50] Solution EPR spectra of **2** (X-band, 25 °C) showed a single unresolved signal at $g_{iso} \sim 1.94$, but the exact g_{iso} value and line width of the signal were significantly solvent-dependent (Table 3 and Figure S10). The solution EPR spectra of **2** (Table 3) were markedly different from those of typical Cr(V) monooxo complexes ($g_{iso} \sim 1.98$; line widths, $\sim 1 \times 10^{-4}$ cm^{-1}).[1,51] Electronic spectra of **2** in polar aprotic solvents (MeCN, DMF, DMSO, and sulfolane) were similar ($\lambda_{max} = 410$ nm, $\epsilon_{max} = 6.9 \times 10^2$ M^{-1} cm^{-1}) and differed from the spectrum of the same compound in H_2O (shoulders at ~400 and ~550 nm), as shown in Figures 5

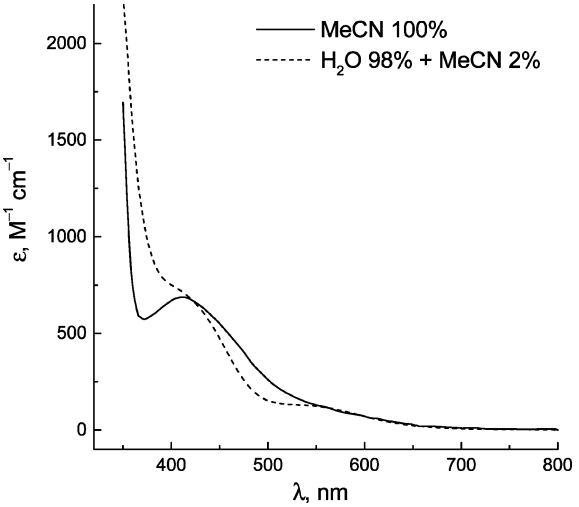

Figure 5. Typical electronic absorption spectra of **2** (0.20 mM) in solutions at 25 °C. (See also Figure S8 in the Supporting Information.) Solvent compositions are given in % v/v.

and S8b−f. Variations in the pH values of aqueous solutions (0.10 M HCl; 0.10 M acetate buffer, pH = 4.0; 0.10 M phosphate buffer, pH = 7.4; 0.10 M NaOH) did not significantly affect the electronic spectra of **2** (Figure S8g−j).

Alternative Methods for the Generation of Cr(V)−phen Complexes. Although **2** was isolated from weakly acidic aqueous solutions (pH ~ 2; see above), the reaction of **1** (1.0 mM) with NaOCl (10 mM) in neutral media (0.10 M phosphate buffer, pH 7.4, ~1 min at 25 °C) also led to quantitative formation of $[Cr^V(O)_2(phen)_2]^+$, which was stable in solution for at least 15 min (determined by electronic and EPR spectroscopies). However, this reaction was strongly inhibited by organic buffers such as HEPES (0.10 M, pH = 7.4, ~10% yield of Cr(V)) or AcOH/NH_3 (0.10 M, pH = 7.4, no formation of Cr(V)).

Oxidation of **1** with PbO_2 in weakly acidic aqueous solutions was studied under the conditions previously used in the generation of Cr(V)−phen species for biological activity studies[5,6] or in the reported isolation of a Cr(V)−phen complex.[16] The reaction of **1** (1.0 mM) with PbO_2 (4-fold molar excess) in AcOH/NH_3 buffer (50 mM, pH = 3.4) for 1 h at 37 °C[5,6] led to a mixture of Cr(V)−phen and Cr(III)−phen species in ~1:4 molar ratio, as shown by ESMS (Figures 3d and S2b; simulation results in Figure 3d are for 22% mol $[Cr^V(O)_2(phen)_2]^+$ and 78% mol $[Cr^{III}(OH)_2(phen)_2]^+$). Isolation of the oxidation products of **1** by perchlorate precipitation (see Experimental Section)[16] led to a mixture of Cr(V)−phen and Cr(III)−phen complexes in ~1:1 molar ratio, according to ESMS of a freshly prepared solution of the isolated solid in MeCN (~0.5 mg mL^{-1}; Figures 3e and S3a; simulation results in Figure 3e are for 50% mol $[Cr^V(O)_2(phen)_2]^+$ and 50% mol $[Cr^{III}(OH)_2(phen)_2]^+$). The presence of significant amounts of Cr(VI) species in the isolated solid was also shown by ESMS (Figure S3a; signals at m/z = 528.1 and 546.1 correspond to $[Cr^{III}(Cr^{VI}O_4)(phen)_2]^+$ and $[Cr^{III}(OH)(HCr^{VI}O_4)(phen)_2]^+$, Table S1 and Figure S7).

Repeated attempts were made to isolate a pure Cr(V)−phen complex from the reactions of **1** with iodosobenzene

(50) Andriessen, W. T. M.; Groenewege, M. P. *Inorg. Chem.* **1976**, *15*, 621−626.
(51) Barr-David, G.; Charara, M.; Codd, R.; Farrell, R. P.; Irwin, J. A.; Lay, P. A.; Bramley, R.; Brumby, S.; Ji, J.-Y.; Hanson, G. R. *J. Chem. Soc., Faraday Trans.* **1995**, *91*, 1207−1216.

(PhIO) in nonaqueous solutions, similar to the method of synthesis of $[Cr^{V}O(salen)]^{+}$ from *trans*-$[Cr^{III}(salen)(OH_2)_2]^{+}$ ($salenH_2$ = *N*,*N*′-bis(salicylidene)-1,2-ethanediamine).[52] Oxidation of **1** with PhIO was also mentioned as a possible route to a Cr(V)−phen complex.[16] Oxidations of **1** with 0.50−5.0 molar equiv of PhIO in MeCN or DMF solutions led to the formation of mixtures of Cr(V), Cr(III), and Cr(VI) products, as detected by ESMS (similar to that in Figures 3e and S3a). Notably, isolation of the oxidation products under certain conditions (such as those described in the Experimental Section) led to the detection of Cr(IV) species (m/z = 445.1, corresponding to $[Cr^{IV}O(OH)(phen)_2]^{+}$) in freshly prepared solutions of the isolated solid in MeCN (∼0.5 mg mL^{-1}; Figures 3f and S3b). Simulation results in Figure 3f are for 45% mol $[Cr^{V}(O)_2(phen)_2]^{+}$, 20% mol $[Cr^{IV}O(OH)(phen)_2]^{+}$, and 35% mol $[Cr^{III}(OH)_2(phen)_2]^{+}$.

Although Cr(V) complexes are commonly generated by the reductions of Cr(VI) in the presence of Cr(V)-stabilizing ligands or by ligand-exchange reactions with Cr(V) 2-hydroxycarboxylato complexes,[1,51,53] all the attempts to produce a Cr(V)−phen complex by one of these methods (Table S2 in Supporting Information) were unsuccessful, as yet.

Reactivity of 2. In a marked contrast with well-studied Cr(V) 2-hydroxycarboxylato complexes, such as $[Cr^{V}O(ehba)_2]^{-}$, which are stable for weeks in aprotic solvents (particularly in DMF or DMSO) and decompose within minutes in aqueous solutions (particularly at pH < 3 or pH > 5),[22,54−56] **2** was equally or more stable in aqueous media compared with nonaqueous solutions (Table 3; the values correspond only to [Cr] = 1.0 mM and 25 °C and are likely to be concentration dependent). Furthermore, it decomposed ∼10 times faster in DMF or DMSO than in MeCN (Table 3). No dramatic changes in the stability of **2** were observed in aqueous solutions over a wide range of pH values (from 0.10 M HCl to 0.10 M NaOH, Table 3).

Formation of Cr(VI) during the decomposition of **2** in various solvents was evident from the increases in absorbance with λ_{max} = 350 or 372 nm (for $[HCrO_4]^{-}$ or $[CrO_4]^{2-}$, respectively)[57] in the electronic absorption spectra (Figure S8). The Cr(VI)/Cr(III) ratio in the decomposition products of Cr(V) is indicative of the relative importance of disproportionation (eq 1) and ligand/solvent oxidation (eq 2) pathways of Cr(V) decomposition (the highest amount of formed Cr(VI), 66.7% mol of the total Cr, is characteristic for the pure disproportionation reaction).[54]

$$3Cr(V) \rightarrow 2Cr(VI) + Cr(III) \quad (1)$$

$$Cr^{V}{=}O + S \rightarrow Cr(III) + SO \quad \text{(where S is an organic substrate)} \quad (2)$$

Concentrations of Cr(VI) after the complete decomposition of **2** ($t \sim 10t_{1/2}$) in various solvents, determined by the DPC method[25,26] (Table 3), indicate that the decomposition of **2** occurs by a combination of both pathways. As for the previously studied Cr(V) complexes,[54−56,58] the disproportionation pathway (eq 1) became more important with an increase in basicity of aqueous solutions (Table 3). Fresh solutions of **2** (in all the studied solvents, Table 3) did not react with DPC (again in a marked contrast with $[Cr^{V}O(ehba)_2]^{-}$, which readily reacts with DPC),[59] so that the increases in the amounts of Cr(VI) generated could be followed as the decomposition of **2** progressed. Reactions of the decomposition products of **2** with DPC revealed a significant difference for such products formed in aqueous or nonaqueous solutions (in all cases, the reactions with DPC were carried out in acidic aqueous solutions; see Experimental Section). Reactions with DPC for the Cr(VI) products formed during the decomposition of **2** in aqueous solutions (regardless of the pH value) were complete within ∼1 min at 25 °C, while those for the Cr(VI) products formed in organic solvents (listed in Table 3) occurred over ∼30 min (typical kinetic curves are shown in Figure S11, Supporting Information).

Typical ESMS spectra of decomposed solutions of **2** in MeCN or H_2O (positive- and negative-ion modes) are shown in Figures S4 and S5. The main stable decomposition product of **2** in MeCN was characterized by a signal at m/z = 528.1, corresponding to $[Cr^{III}(Cr^{VI}O_4)(phen)_2]^{+}$ (Figures S4a and S7), and no signals, apart from those of BF_4^{-}, were observed in the negative-ion mode (Figure S5a). Decomposition of **2** (1.0 mM) in H_2O solution led to the appearance of signals due to $[Cr^{III}(OH)_2(phen)_2]^{+}$, $[Cr^{III}(Cr^{VI}O_4)(phen)_2]^{+}$, and $[Cr^{III}(OH)(HCr^{VI}O_4)(phen)_2]^{+}$ (m/z = 446.1, 528.1, and 546.1, respectively, Figure S4b), as well as of that due to $[HCr^{VI}O_4]^{-}$ (m/z = −117.1) in the negative-ion mode (Figure S5b). Small amounts of $[Cr^{IV}(O)(OH)(phen)_2]^{+}$ (m/z = 445.1) were detected at the late stages of the decomposition of **2** in MeCN but not in H_2O (insets in Figure S4a,b). Aqueous solutions containing **1** and $[CrO_4]^{2-}$ (0.50 mM each) produced comparably intense ESMS signals at m/z = 446.1, 528.1, and 546.1 (which are similar to the decomposition products of **2** in H_2O), but the m/z = 528.1 signal became dominant with an increase in capillary temperature and cone voltage (Figures S6a,b).

Dissolution of **2** (1.0 mM) in aqueous solutions of typical Cr(V)-stabilizing ligands,[51,53] such as $ehbaH_2$/ehbaH (0.10 mM in H_2O, pH = 3.5) or D-glucose (0.50 M, in 0.10 M phosphate buffer, pH = 7.4) at 25 °C led to slow ligand-exchange reactions (hours time scale, observed by EPR spectroscopy, Figure S12 in Supporting Information), resulting in the formation of well-characterized complexes,[51]

(52) (a) Srinivasan, K.; Kochi, J. K. *Inorg. Chem.* **1985**, *24*, 4671−4679. (b) Samsel, E. G.; Srinivasan, K.; Kochi, J. K. *J. Am. Chem. Soc.* **1985**, *107*, 7606−7617.
(53) Codd, R.; Dillon, C. T.; Levina, A.; Lay, P. A. *Coord. Chem. Rev.* **2001**, *216−217*, 533−577 and references therein.
(54) Krumpolc, M.; Roček, J. *Inorg. Chem.* **1985**, *24*, 617−621.
(55) Codd, R.; Levina, A.; Zhang, L.; Hambley, T. W.; Lay, P. A. *Inorg. Chem.* **2000**, *39*, 990−997.
(56) Levina, A.; Lay, P. A.; Dixon, N. E. *Inorg. Chem.* **2000**, *39*, 385−395.
(57) Brasch, N. E.; Buckingham, D. A.; Evans, A. B.; Clark, C. R. *J. Am. Chem. Soc.* **1996**, *118*, 7969−7980.
(58) Levina, A.; Zhang, L.; Lay, P. A. *Inorg. Chem.* **2003**, *42*, 767−784.
(59) Eckert, J. M.; Judd, R. J.; Lay, P. A.; Symons, A. D. *Anal. Chim. Acta* **1991**, *255*, 31−33.

Table 4. XANES Spectroscopic Parameters of Cr(V/IV/III)−phen Complexes (Solids, 10 K) in Comparison with Those of Cr(V/IV/III)−ehba Complexes[62]

	oxidation state					
	Cr(V)		Cr(IV)		Cr(III)	
ligand[a]	phen	ehba	phen	ehba	phen	ehba
edge,[b] eV	6002.4	6004.5	6001.8	6003.7	5998.9	6003.0
preedge, eV	5992.8	5992.5	5990.4,[d] 5992.8	5990.1,[d] 5991.5, 5992.7	5987.2, 5990.0[d]	5990.7, 5992.7
preedge/edge[c]	0.33	0.41	0.03,[d] 0.11	0.03,[d] 0.09	0.025, 0.028	0.038, 0.025

[a] Structures of the complexes: $[Cr^{V}O(ehba)_2]^-$, $[Cr^{IV}O(ehbaH)_2]^0$, and $[Cr^{III}(ehbaH)_2(OH_2)_2]^+$;[62] $[Cr^{V}(O)_2(phen)_2]^+$ (**2**), $[Cr^{IV}(O)(OH)(phen)_2]^+$ (**3**); $[Cr^{III}(phen)_2(OH_2)_2]^{3+}$ (**1**). [b] Edge energy determined at 50% of the edge jump. [c] Intensities of the preedge absorbancies relative to the edge jump. [d] Shoulder.

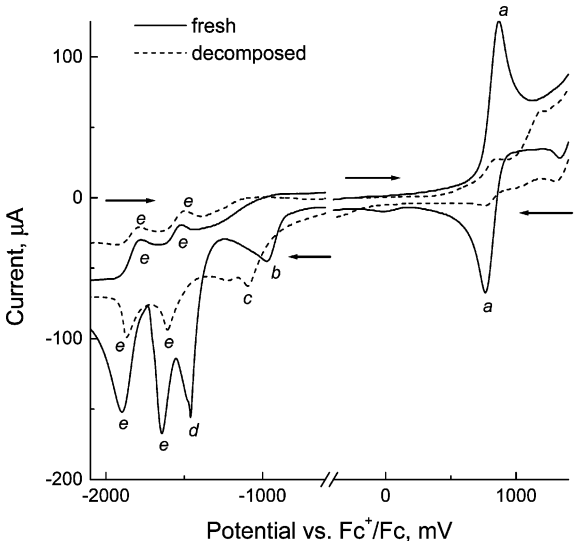

Figure 6. Typical cyclic voltammograms of fresh and decomposed (24 h at 25 °C) solutions of **2** ([Cr] = 5.0 mM) in MeCN (containing 0.10 M $(^nBu_4N)BF_4$ as a supporting electrolyte) at 25 °C on a glassy carbon electrode with scan rate 100 mV s^{-1} and 100% *iR* compensation. Assignment of the signals (see Discussion): a is the couple associated with the oxidation of Cr(V), b is due to the Cr(V) → Cr(IV) conversion, c is due to the Cr(III) → Cr(II) conversion, d is due to the Cr(IV) → Cr(III) → Cr(II) conversion, and e signals are due to the metal-assisted ligand reductions. Directions of the scans are shown with arrows.

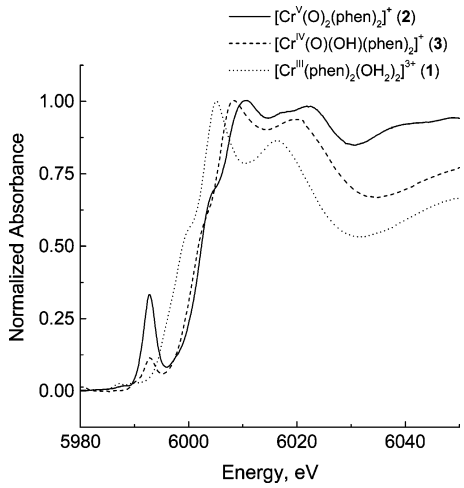

Figure 7. XANES spectra of Cr(V/IV/III)−phen complexes. The structure of $[Cr^{IV}O(OH)(phen)_2]^+$ was assigned on the basis of ESMS and XAFS data (see Discussion). Parameters of the spectra are listed in Table 4. All the spectra were acquired from solid mixtures with BN (∼1:1 w/w) at 10 K.

$[Cr^{V}O(ehba)_2]^-$ ($g_{iso} = 1.9782$, $A_{iso} = 17.1 \times 10^{-4}$ cm^{-1}) or $[Cr^{V}O(L)_2]^-$ (LH_2 = D-glucose, $g_{iso} \sim 1.980$ for a mixture of linkage isomers). Like $[Cr^{V}O(ehba)_2]^-$,[60] **2** was reduced rapidly (within ∼10 s at 25 °C and [Cr] = 1.0 mM) and quantitatively to Cr(III) by stoichiometric amounts of glutathione (2.0 mM, one-electron reductant) or ascorbate (1.0 mM, two-electron reductant) in neutral aqueous solutions (0.10 M phosphate buffer, pH = 7.4). Electronic absorption spectra of the reduction products of **2** (λ = 350−800 nm) were not significantly different from those of **1** in the same buffer. Reactions of **2** with 0.2−0.5 molar equiv of glutathione or ascorbate in H_2O (the pH value was adjusted to ∼7.4 by addition of NaOH), followed by ESMS, showed the formation of mixtures of Cr(V)−phen and Cr(III)−phen, but not Cr(IV)−phen, complexes. Notably, **2** was rapidly reduced (within ∼5 min at 25 °C and [Cr] = 1.0 mM) by a commonly used buffer, HEPES (0.10 M, pH 7.4), while $[Cr^{V}O(ehba)_2]^-$ did not react with HEPES under these conditions.[56]

Redox reactions of **2** in MeCN ([Cr] = 5.0 mM, 25 °C, using 0.10 M $(^nBu_4N)BF_4$ as a supporting electrolyte) were followed by cyclic voltammetry, in comparison with those of a decomposed (24 h at 25 °C) solution of **2** (Figure 6). A quasi-reversible oxidation (a in Figure 6, $E_{1/2}$ = 795 mV vs Fc^+/Fc, ΔE_p = 100 mV) and an irreversible reduction (b in Figure 6, E_{max} = −970 mV) were characteristic for fresh solutions of **2**, while several irreversible or quasi-reversible reductions at $E < -1.0$ V (c−e in Figure 6) were observed in both the fresh and decomposed solutions. No significant redox responses were observed for the solutions of phen (10 mM) in MeCN under the same conditions.

X-ray Absorption Spectroscopy of 1−3. Changes in the X-ray absorption near-edge (XANES) spectra of Cr(V/IV/III)−phen complexes (Figure 7 and Table 4), including the increases in edge energy and in the intensity of preedge absorbance (due to a symmetry-forbidden 1s → 3d transition)[61] with an increase in Cr oxidation state, were similar to those for the Cr(V/IV/III)−ehba series (Table 4).[62] The energies and intensities of the preedge absorbances were similar for both redox series, while the edge positions for the Cr(V/IV/III)−phen complexes were shifted to lower energies by 2−4 eV compared with the corresponding ehba complexes (Table 7).[62]

(60) Lay, P. A.; Levina, A. *J. Am. Chem. Soc.* **1998**, *120*, 6704−6714.

(61) (a) Ellis, P. J.; Joyner, R. W.; Maschmeyer, T.; Masters, A. F.; Niles, D. A.; Smith, A. K. *J. Mol. Catal. A: Chem.* **1996**, *111*, 297−305. (b) Engemann, C.; Hormes, J.; Longen, A.; Dötz, K. H. *Chem. Phys.* **1998**, *237*, 471−481.

(62) Levina, A.; Codd, R.; Foran, G. J.; Hambley, T. W.; Maschmeyer, T.; Masters, A. F.; Lay, P. A. *Inorg. Chem.* **2004**, *43*, 1046−1055.

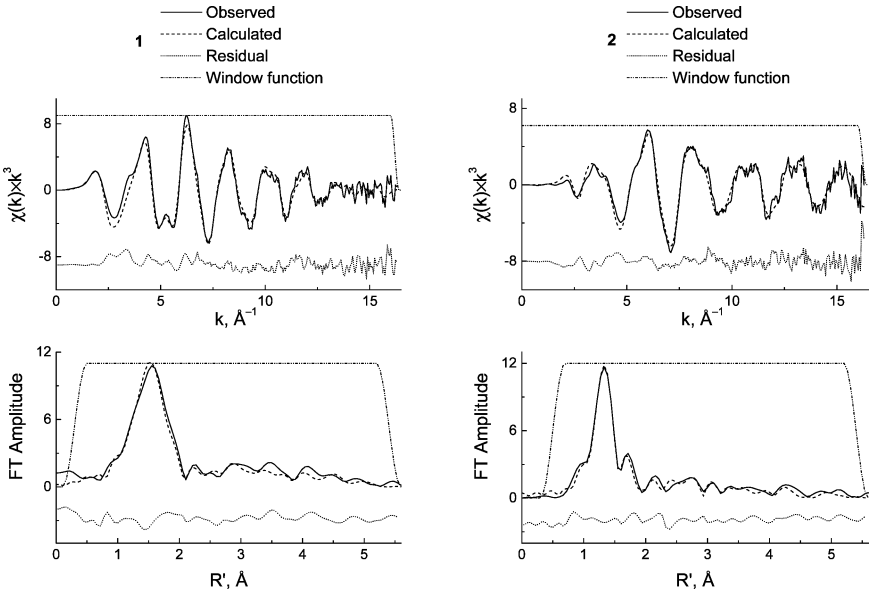

Figure 8. Experimental (solid mixtures with BN, ~1:1 w/w, 10 K) and calculated (MS, models **1** and **2a** in Chart 1) XAFS and FT XAFS spectra of **1** and **2**. Selected fitted parameters are listed in Table 2, and details of the MS XAFS calculations are given in Tables S5−S7, Supporting Information.

Figure 8 presents experimental XAFS and Fourier transformed (FT) XAFS spectra for **1** and **2**, together with their best MS fits (see below). Table S3 (Supporting Information) summarizes the applications of SS XAFS models to the first coordination shells in **1** and **2**. A model derived from the crystal structure of **1** (Figure 1 and Table 2), including two Cr−O bonds at 1.94 ± 0.01 Å and four Cr−N bonds at 2.06 ± 0.01 Å, resulted in a good fit for **1** (R = 14.0%, Table S3, fits with R < 20% are considered acceptable).[30] Application of the same model for **2** resulted in the optimized bond lengths of 1.62 ± 0.01 Å and 2.10 ± 0.01 Å for the Cr−O and Cr−N bonds, respectively (R = 10.3%, Table S3). A significant increase in the Debye−Waller factor (σ^2) value for Cr−N bonds in **2** (0.0085 Å^2, Table S3) compared with that for **1** (0.0018 Å^2) suggested a higher degree of disorder in these bonds. No significant improvements of the SS XAFS fits for **2** were achieved by using more complex models (e.g., those with two different types of Cr−O or Cr−N bonds).

The best SS XAFS fit for **3** (Table 2 and Figure S13 in Supporting Information) included one Cr−O bond at 1.54 ± 0.01 Å, one Cr−O bond at 1.70 ± 0.01 Å, and four Cr−N bonds at 2.02 ± 0.01 Å (details of the calculations are given in Table S4, Supporting Information). Application of a model with two equal Cr−O bonds (average length, 1.62 Å, Table S4) to SS XAFS calculations for **3** resulted in a statistically significant[34,35] deterioration of the fit (R = 20.6 vs 11.8%, models A and C in Table S4). The difference in lengths of the two types of Cr−O bonds in **3** (0.16 Å, Table 2) exceeds the resolution limit (0.12 Å) for SS XAFS calculations at k = 0−13 Å^{-1} (Figure S13)[17,29] and, hence, is meaningful.

Selected structural parameters of the fitted MS XAFS models of **1** and **2** are listed in Table 2, and details of the MS XAFS calculations are shown in Tables S5−S7, Supporting Information. Application of a MS XAFS model for **1**, including all non-hydrogen atoms in *cis*-[Cr^{III}(phen)$_2$(OH$_2$)$_2$]$^+$ (derived from the crystal structure), led to a good fit (R = 17.5%, Figure 8). All the values of bond lengths and angles in the fitted MS XAFS model of **1** were within 0.02 Å or 5°, respectively, of those found by X-ray crystallography (Table 2; see also Table S6 and the attached CIF file). Inclusion of four additional oxygen donors, bound to the aqua ligands of **1** by hydrogen bonds (Figure 2), into the MS XAFS model (the O···O distances were restrained at 2.60 ± 0.05 Å, in agreement with the crystal structure), led to a slight improvement in the fit (R = 16.4%), but this was not statistically significant (according to the F-test).[34,35]

The main conditions used in the MS XAFS model of **1** (Table S5) were the following. (i) All the bond lengths and angles within the phen ligands were restrained (within 0.02 Å or 2°, respectively) to those found in the crystal structure (see the attached CIF file). (ii) The phen ligands were restrained to be planar (within 0.1°). (iii) The two phen ligands were set to be equal (using coordinate and σ^2 value constraints), which led to a significant decrease in the number of varied parameters.[33] (iv) The phen ligands were not assumed to be totally internally symmetrical, due to the different locations of the two *N*-donors of each ligand in the complex (cis or trans in relation to the O-donors; **1** in Chart 1). (v) No restraints were applied to the O-donors. Since this model was successfully used for **1** (as verified by comparison with the crystal structure, Table 2), it was applied without change to the MS XAFS modeling for **2**, which resulted in a good fit (R = 18.1% for **2a** in Chart 1, Figure 8). Details of the fitted parameters are given in Table S6, and the most significant scattering paths for this model are listed in Table S7.

The main differences in the fitted parameters for **2**, compared with those for **1** (Tables 2 and S6) were the following: (i) a decrease in the Cr−O bond lengths from 1.94 to 1.63 Å, consistent with the formation of Cr−oxo triple[63] bonds (as well as with the results of SS XAFS modeling, Table S3); and (ii) a significant difference in the lengths of Cr−N bonds in the cis or trans positions in relation

to the oxo ligands (2.16 or 2.04 Å, respectively, **2a** in Chart 1). A model with "reversed" Cr−N bonds (**2b** in Chart 1) resulted in an equally good fit (R = 18.1%, Table S6). However, restraining the two Cr−N bonds in each phen ligand to be equal (within 0.05 Å) led to a poor fit (R = 23.4%) and to unreasonably high σ^2 values ($\geq$0.02 Å^2) for some of the atoms in the ligands (Table S6). Application of a model with *trans*-oxo groups (**2c** in Chart 1, no restraints on Cr−N bonds) also resulted in a relatively poor fit (R = 19.8%) and unreasonably high σ^2 values (Table S6).

Discussion

Purity and Structure of 2. The purity of the isolated complex **2** was confirmed by elemental analyses, ESMS (Figure 3), magnetic susceptibility measurements, solid-state EPR spectroscopy (showing the absence of Cr(III) impurities, Figure 4), and the lack of reactivity with DPC for fresh solutions of **2** (showing the absence of Cr(VI) impurities). By contrast, the previously described method for the isolation of $[Cr^V(O)_2(phen)_2]^+$ (oxidation of **1** with PbO_2, followed by perchlorate precipitation)[16] led to a mixture of Cr(III), Cr(V), and Cr(VI) species (as determined by ESMS, Figures 3e and S3a). The XANES spectrum of **2** (Figure 7) is consistent with the Cr(V) oxidation state of the metal ion; a shift in the edge position to lower energies compared with that for $Na[Cr^VO(ehba)_2]$ (Table 4)[62] is explained by the weaker donor properties of the phen ligands compared with those of the ehba ligands, as was observed previously for a Cr(V)−glutathione complex.[58] A decrease in the preedge absorbance intensity in the XANES spectrum of **2** compared with that of $[Cr^VO(ehba)_2]^-$ (Table 4)[62] is consistent with an increase in coordination number of Cr from 5 to 6.[64]

Significant decomposition of **2** occurs within several hours at 25 °C in both aqueous and nonaqueous solvents (Table 3), which makes it very difficult to grow crystals of this compound that are suitable for X-ray crystallography. Therefore, as for many other Cr(V) complexes,[1,17] XAFS data analysis is the only readily accessible method for the structural characterization of **2**. Analysis of XAFS data, using both the SS and MS models (Figure 8 and Tables 2 and S3−S7), confirmed the previously assigned[16] *cis*-$[Cr^V(O)_2(phen)_2]^+$ structure for **2**, which makes it the first structurally characterized Cr(V) dioxo complex.[4] Another reported complex, $[Co^{III}Cp_2][Cr^V(O)_2(NRAr)_2]$ (Cp = cyclopentadienyl(1−), R = $C(CD_3)_2CH_3$, and Ar = 2,5-C_6H_3FMe), has been characterized by ^{2}H NMR spectroscopy and magnetic measurements.[65] The distorted octahedral structure of **2** is also unusual for Cr(V) oxo complexes (most of which are five-coordinate with square-pyramidal or trigonal-bipyramidal geometries).[4,66] The validity of the MS model used to determine the structure of **2** was confirmed by successful application of the same model to XAFS data analysis for a closely related complex **1** that was characterized by X-ray crystallography.

The Cr═O bonds in **2** (1.63 Å, Table 2) are longer than those for typical Cr(V) monooxo complexes (~1.55 Å)[66] and close to those in $[Cr^VO(LH_2)_2]^{3-}$ (LH_5 = glutathione, 1.61 Å, determined by MS XAFS calculations).[58] It is likely that the increased bond length in the phen complex compared to other complexes with only N- and O-donors, arises from the sharing of one of the metal t_{2g} orbitals involved in forming one of the two π bonds involved in each of the Cr≡O triple bonds.[63] The average Cr−N bond lengths in **2** (2.10 Å, determined by SS XAFS modeling, Table S3) are slightly larger that those in **1** (2.06 Å, Table 2) and close to those for the Cr(V)−N(pyridine) bonds (2.085 Å) in a crystallographically characterized complex, $[Cr^V(N)(bpb)]^0$ (H_2bpb = 1,2-bis(2-pyridinecarboxamido)benzene).[67] The MS XAFS analysis revealed a significant difference in the two Cr−N bond lengths involving each of the phen ligands in **2** (2.04 and 2.16 Å, Table 2), which is consistent with the relatively high σ^2 values for these bonds in the SS XAFS model (Table S3). Although the MS XAFS calculations did not distinguish between the structures **2a** and **2b** (Chart 1), the former is likely to be more energetically favorable, due to the steric demands of the two oxo groups (a space-filling model, based on the optimized structure **2a**, is shown in Figure S14, Supporting Information). A significant difference in the Cr−N bond lengths in **2** is likely to lead to a very complex ^{14}N superhyperfine coupling pattern in solution EPR spectra due to two sets of two equivalent ^{14}N atoms, which is responsible for the observed broad EPR signals with no resolved superhyperfine structures (Table 3 and Figure S10). By contrast, well-resolved ^{14}N superhyperfine couplings are observed for square-planar Cr(V) complexes with tetradentate N-donor ligands, where all the Cr−N bonds are equivalent.[52,67−71] The *trans*-dioxo structure **2c** (Chart 1) is unlikely, on the basis of the results of MS XAFS modeling (Table S6) and IR-spectroscopic data (Figure S9).[16] Structure **2c** is also inconsistent with the rapid formation of **2** by hypochlorite oxidation of a *cis*-diaquachromium(III) complex, **1**, and its rapid reduction to the same Cr(III) complex by ascorbate or glutathione (on the basis of the electronic absorption spectroscopy data; see Results).

Solution Chemistry of 2 and the Formation of Cr(IV) Intermediates. In line with its unusual structure, the reactivity of **2**, particularly its stability patterns in various solvents (Table 3), differs markedly from those of classical Cr(V) complexes such as $[Cr^VO(ehba)_2]^-$.[22,56] In addition, unlike most of the known Cr(V) complexes,[51,53,66] **2** could only be formed to date by oxidation of a corresponding Cr(III)

(63) Although the Cr(V)−oxo bonds are traditionally represented as double bonds (e.g., in Chart 1 or in ref 4), it is more correct to consider them as triple bonds, including one σ and two orthogonal π bonds. This is also consistent with the very short bond lengths.

(64) Aitken, J. B.; Thomas, S. E.; Stocker, R.; Thomas, S. R.; Takikawa, O.; Armstrong, R. S.; Lay, P. A. *Biochemistry* **2004**, *43*, 4892−4898.
(65) Odom, A. L.; Mindiola, D. J.; Cummins, C. C. *Inorg. Chem.* **1999**, *38*, 3290−3295.
(66) Farrell, R. P.; Lay, P. A. *Comments Inorg. Chem.* **1992**, *13*, 133−175.
(67) Che, C. M.; Ma, J. X.; Wong, W. T.; Lai, T. F.; Poon, C. K. *Inorg. Chem.* **1988**, *27*, 2547−2548.
(68) Collins, T. J.; Slebodnick, C.; Uffelman, E. S. *Inorg. Chem.* **1990**, *29*, 3433−3436.
(69) Meier-Callahan, A. E.; Gray, H. B.; Gross, Z. *Inorg. Chem.* **2000**, *39*, 3605−3607.
(70) Headlam, H. A.; Lay, P. A. *Inorg. Chem.* **2001**, *40*, 78−86.
(71) Barnard, P. J. Ph.D. Thesis, University of Sydney, 2002.

Scheme 1. Formation and Hydrolysis of a Cr(III)−Cr(VI) Dimer **4** in Decomposed Solutions of **2**

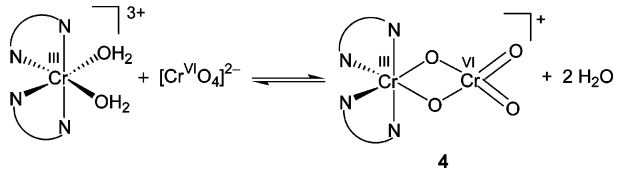

4

complex (**1**) and not by reduction of Cr(VI) in the presence of phen ligand (Table S2).

The ESMS of decomposed solutions of **2** in MeCN (Figures S4a and S5a) show the formation of a Cr(III)−Cr(VI) dimer ($m/z = 528.1$, proposed structure **4** in Scheme 1) as a main Cr product. Although the same species can be formed in the gas phase during the ESMS of aqueous solutions containing **1** and $[CrO_4]^{2-}$ (Figure S6), the presence of **4** in solutions after the decomposition of **2** in organic solvents is evident from the slow reactions with DPC (Figure S11), due to gradual release of Cr(VI) from a kinetically inert complex with Cr(III) (**4**).[4] Similar kinetics were previously observed for the reactions of Cr(III)-bound thiolato ligands with Ellman's reagent (a specific reagent for thiols).[26] During the decomposition of **2** in aqueous solutions, the initially formed **4** is likely to undergo hydrolysis with the formation of $[Cr^{III}(phen)_2(OH_2)_2]^{3+}$ and $[Cr^{VI}O_4]^{2-}$ (Scheme 1, consistent with the ESMS data in Figures S4−S6).

Decomposition of $[Cr^{V}(O)_2(phen)_2]^{+}$ in nonaqueous solutions, particularly at high Cr concentrations, also leads to the formation of a Cr(IV) intermediate ($[Cr^{IV}(O)(OH)(phen)_2]^{+}$ according to ESMS), as shown by the isolation of a Cr(IV)-containing solid (**3**) after the oxidation of **1** with PhIO in MeCN/DMF solution (Figures 3f and S3b), as well as by the detection of traces of Cr(IV) in the decomposition products of **2** (1.0 mM) in MeCN (Figure S4a). By contrast, no detectable amounts of Cr(IV) intermediates were formed during the decomposition or reduction of **2** in aqueous solutions. The results of XANES spectroscopy (Figure 7) and SS XAFS analyses (Table S4 and Figure S13) for **3** are consistent with $[Cr^{IV}O(OH)(phen)_2]^{+}$ being the predominant Cr species in the solid state. The Cr−ligand bond lengths in **3**, determined by SS XAFS analyses (Tables 2 and S4), are close to those in structurally characterized Cr(V) complexes with oxo, alkoxo, and imine donors, respectively.[65,72] The XANES spectrum of **3** (Figure 7) cannot be due to a mixture of Cr(III) and Cr(V) species as, if this was the case, a decrease in the preedge absorbance would match a shift in the edge energy.[73] The ESMS results for a solution of **3** in MeCN that show the presence of a mixture of Cr species in the oxidation states from +III to +VI (Figures 3f and S3b) are likely to be due to the rapid decomposition of $[Cr^{IV}O(OH)(phen)_2]^{+}$ in solution and/or in the gas phase. No further characterization of **3** was performed due to the low yields of the solid (see Experimental Section).

A quasi-reversible oxidation of $[Cr^{V}(O)_2(phen)_2]^{+}$ in MeCN solution (a in Figure 6) may lead either to $[Cr^{VI}(O)_2(phen)_2]^{2+}$ or to $[Cr^{V}(O)_2(phen)(phen^{\bullet+})]^{2+}$, by analogy with the redox chemistry of Cr−porphyrin complexes.[74] An irreversible reduction at −850 to −1200 mV (b in Figure 6) is likely to be due to a Cr(V) → Cr(IV) redox reaction. Quasi-reversible or irreversible electrochemical reductions at $E \sim -1.0$ V (vs Fc^{+}/Fc, in MeCN or DMF solutions) are characteristic for Cr(V) complexes with N- and/or O-donor ligands.[22,71] The irreversible reduction of Cr(V) to Cr(IV) is consistent with the observed low stability of Cr(IV)−phen species in solutions. Multiple reduction signals at $E < -1.0$ V (c−e in Figure 6) are similar to those observed for Cr(III) complexes with aromatic imine ligands[75] and correspond to the Cr(III) → Cr(II) conversion (c and d in Figure 6), as well as to the metal-assisted ligand reduction (e in Figure 6).[75]

Implications for Cr-Induced Genotoxicity. Oxidations of **1** by either NaOCl (in H_2O) or PbO_2 (in aqueous acetate buffers, pH 3−4) lead to $[Cr^{V}(O)_2(phen)_2]^{+}$ as the main oxidation product, as shown by ESMS (Figures 3b,d, S1b, and S2b), EPR spectroscopy (Table 3 and Figure S10), and electronic absorption spectroscopy (Figure S8). This means that $[Cr^{V}(O)_2(phen)_2]^{+}$ was responsible for the oxidative DNA damage in vitro, bacterial mutagenicity, and increased incidence of micronuclei in mammalian cells, caused by the reaction mixture after the oxidation of **1** with PbO_2.[5,6] Decomposition of $[Cr^{V}(O)_2(phen)_2]^{+}$ in aqueous solutions was slow on the time scale of the biological tests (Table 3).[5,6] It is also likely that the formation of $[Cr^{V}(O)_2(phen)_2]^{+}$ during the extra- or intracellular oxidation of **1** causes the increased mutagenicity and genotoxicity of **1** compared with most Cr(III) compounds.[5,11]

This work has shown for the first time that **1** can be rapidly oxidized to a Cr(V) complex in neutral aqueous solutions by a biological oxidant, hypochlorite (ClO^{-}).[76] Although in biological systems ClO^{-} is more likely to react with more abundant organic compounds,[77] as confirmed by strong inhibition of the formation of $[Cr^{V}(O)_2(phen)_2]^{+}$ by organic buffers, oxidation of Cr(III) to Cr(V) may also potentially be performed by secondary oxidants, such as chloramines, formed in the reactions of ClO^{-} with amino acids and other common biomolecules.[78] The isolated complex **2** is more stable in neutral aqueous solutions ($t_{1/2} \sim 5$ h at 25 °C, Table 3) than most of the previously studied Cr(V) complexes,[54−56,58] except for those with macrocyclic ligands.[79] Complex **2** is rapidly reduced by common biological reductants, ascorbate and glutathione (see Results), as are other biologically active

(72) Headlam, H. A.; Weeks, C. L.; Turner, P.; Hambley, T. W.; Lay, P. A. *Inorg. Chem.* **2001**, *40*, 5097−5105.
(73) Cawich, C. M.; Ibrahim, A.; Link, K. L.; Bumgartner, A.; Patro, M. D.; Mahapatro, S. N.; Lay, P. A.; Levina, A.; Eaton, S. S.; Eaton, G. R. *Inorg. Chem.* **2003**, *42*, 6458−6468.
(74) Guldi, D. M.; Neta, P.; Hambright, P. *J. Chem. Soc., Faraday Trans.* **1992**, *88*, 2013−2019.
(75) Hughes, M. C.; Macero, D. J. *Inorg. Chem.* **1976**, *15*, 2040−2044.
(76) Halliwell, B. In *Active Oxygen in Biochemistry*; Valentine, J. S., Foote, C. S., Greenberg, A., Liebman, J. F., Eds.; Blackie Academic and Professional: London, 1995; pp 313−335.
(77) Pattison, D. I.; Davies, M. J. *Chem. Res. Toxicol.* **2001**, *14*, 1453−1464.
(78) Pattison, D. I.; Davies, M. J.; Asmus, K.-D. *J. Chem. Soc., Perkin Trans. 2* **2002**, 1461−1467.
(79) Dillon, C. T.; Lay, P. A.; Bonin, A. M.; Dixon, N. E.; Collins, T. J.; Kostka, K. L. *Carcinogenesis* **1993**, *14*, 1875−1880.

Cr(V) complexes, including $[Cr^{V}O(ehba)_2]^-$.[60] Additional stabilization of $[Cr^{V}(O)_2(phen)_2]^+$ in biological systems can be provided by ligand-exchange reactions with ubiquitous carbohydrate ligands, such as D-glucose (Figure S12b) or glycoproteins.[80]

Although Cr(III)−phen complexes are not formed in biological systems and are not currently used as nutritional supplements,[1] the chemistry of such species and their Cr(V) analogues under biologically relevant conditions may represent that of Cr(III) and Cr(V) complexes with biological imine ligands, which are likely to form during the intracellular reduction of carcinogenic Cr(VI).[1] Biological oxidation of a popular nutritional supplement, $[Cr^{III}(pic)_3]$ (pic = picolinato(−) = 2-pyridinecarboxylato(−), i.e., an imine-containing ligand), with the formation of Cr(V/IV)−pic intermediates[73,81] is also likely to contribute to the reported genotoxicity of this compound.[82] Oxidation of $[Cr^{III}(pic)_3]$ by H_2O_2 in neutral aqueous media at 37 °C leads to slow (hours time scale) formation of Cr(VI).[7a] Conversion of a stable tris-chelate complex, $[Cr^{III}(pic)_3]$, to more reactive species, such as $[Cr(pic)_2(OH_2)_2]^+$ or $[Cr_2(OH)_2(pic)_4]$,[83,84] may occur in acidic media of the stomach or by enzyme-assisted metabolism in the liver.[85] Systematic studies of the biologically relevant oxidation reactions of $[Cr^{III}(pic)_3]$ and its decomposition products are yet to be performed.

In summary, the results of this work support the hypothesis[1,5,6] that biological oxidative recycling of Cr(III) complexes is involved in the mechanisms of Cr(VI)-induced carcinogenicity and that this also has the potential to lead to adverse health effects caused by excessive use of Cr(III)-containing nutritional supplements.

Acknowledgment. Financial support of this work was provided by Australian Reseach Council (ARC) Large and Discovery grants to P.A.L. including an ARC Australian Professorial Fellowship, an ARC Small grant to R.R.F., ARC RIEFP grants for the X-ray diffractometer and 10-element Ge detector, ESMS equipment, Wellcome Trust and ARC equipment grants for the EPR equipment, and Australian Synchrotron Research program (ASRP) grants for access to the Australian National Beamline Facility (ANBF) in Tsukuba, Japan. The X-ray absorption spectroscopic (XAS) studies were performed at ANBF with support from the ASRP, which is funded by the Commonwealth of Australia under the Major National Research Facilities program. C.L.W. is grateful for funding through the Australian Postgraduate Award. We thank Drs. Garry Foran (ANBF) and Hugh Harris (University of Sydney) for assistance in recording the XAS data, Dr. David Pattison (The Heart Research Institute, Sydney), and Professor Y. Sulfab for helpful discussions.

Supporting Information Available: Figures showing typical ESMS data for **1** and its oxidation products, EPR, IR, and electronic spectra of **2**, kinetics of the reactions of the decomposition products of **2** with DPC, experimental and fitted XAFS spectra for Cr(IV)−phen, and a space-filling model of **2** based on the structure optimized by MS XAFS calculations, tables showing the assignment of major ESMS signals, conditions for the attempted generation of Cr(V)−phen complexes from Cr(VI) or Cr(V) precursors, and details of XAFS fittings for **1**−**3**, and details of the X-ray crystal structure of **1** reported as a CIF file. This material is available free of charge via the Internet at http://pubs.acs.org.

IC049008Q

(80) Codd, R.; Irwin, J. A.; Lay, P. A. *Curr. Opin. Chem. Biol.* **2003**, *7*, 213-219.
(81) Codd, R.; Lay, P. A.; Levina, A. *Inorg. Chem.* **1997**, *36*, 5440−5448.
(82) (a) Stearns, D. M.; Silveira, S. M.; Wolf, K. K.; Luke, A. M. *Mutat. Res.* **2002**, *513*, 135−142. (b) Hepburn, D. D. D.; Xiao, J.; Bindom, S.; Vincent, J. B.; O'Donnell, J. *Proc. Natl. Acad. Sci. U.S.A.* **2003**, *100*, 3766−3771.
(83) Kita, E.; Uscinska, G. *Transition Met. Chem.* **2003**, *28*, 373−380.
(84) Stearns, D. M.; Armstrong, W. H. *Inorg. Chem.* **1992**, *31*, 5178−5184.
(85) Kareus, S. A.; Kelley, C.; Walton, H. S.; Sinclair, P. R. *J. Hazard. Mater.* **2001**, *B84*, 163−174.